Antenna Dome 2.0

Error model for beam-forming system

Bsc Thesis

Bo Wen Xu & Arjan Kamminga

Abstract

A new antenna measurement setup, the Antenna Dome, is being developed, which can provide real time antenna and beamformer measurements. In order to be able to validate this setup, an existing beamforming system will be will be extensively studied and characterized. Multiple measurement setups will be used, providing multiple measured characteristics. The result is an accurate statistical model for the steering system, and a comprehensive error model for the complete beamforming system, including the provided antenna array. This model will help in validating the functionality of the Antenna Dome, and ultimately will help in its further development.

Contents

1

Introduction

With the rapid innovation in 5G technology and new beam-forming capabilities, new challenges arise for current antenna measurement systems. The current systems rely on scanning the beam pattern of the antenna under test (AUT). This is done by scanning arms or rotating scanners that take step-wise measurements of a certain area around the AUT [1]. A single measurement therefore usually takes a couple of minutes. Making multiple measurements for different antenna setups increases the time needed significantly, and high speed beam switching cannot be properly measured with such a system. These high speed AUT measurements are important for testing spatial multiplexing systems, which have beam switching times below 1 second.

To tackle these challenges, a new measurement system is being developed at the TU Delft called the Antenna Dome. The Antenna Dome is a spherical chamber where several receiver antennas jointly measure the radiation pattern of an AUT. The dome consists of a aluminium skeleton covered by 3D-printed panels that form an outer shell as can be seen in figure 1.1. The outer shell has a layer of absorbing material on the inside (pre-made pads or paints) and forms a half-sphere. This half-sphere shields the measurement setup from external EM waves and noise and absorbs reflected waves from inside. The multiple antenna's and sensing nodes make it possible to measure the AUT in real-time. No scanning or movement is required as all antenna's measure the radiation pattern at the same time. No Network Analyzer is required either, as the sensing nodes directly measure the amplitude at the node and send it to the processing system. At this moment, only the amplitude, and not the phase of the radiated field can be measured.

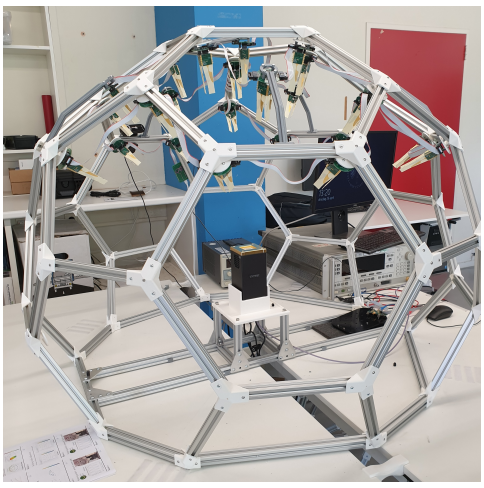

Figure 1.1: Antenna Dome 1.0 (without outer panels)

For the development of the Antenna Dome, multiple individual technologies must first be developed and tested, such as the development of new sensing nodes and testing absorbing material options. Most importantly, a way of calibrating the Antenna Dome and validating its functionality must be developed. To validate the functionality, an existing beam-forming system will be accurately studied and characterized. A standard deviation model and error model will be developed for the system, which can be used as a benchmark for Antenna Dome measurements. The chosen beam-forming system is the BBox One 5G 28GHz from TMYTEK [2]. It is a non-IC beam-forming development tool that can be used to test different antenna arrays. The system was readily available, and it provides both a useful validation system and future functionality for testing antenna's.

The purpose of this thesis is to show the design procedure of the error model. First, a measurement setup and procedure must be developed to provide a simple and effective way of carrying out multiple measurements. S-parameter behavior of the beam-forming system will be measured extensively using a PNA. The gathered data will be used to develop a deviation and statistical model of the BBox behavior. These models will be verified through multiple random measurements. The provided antenna array will then be characterized with near field (NF) measurements. Both single element and total array measurements will be carried out. This antenna model can then be combined with the statistical model to create a comprehensive error model for the whole beam-forming system. Finally, this model will be tested and validated by conducting multiple measurements, including Antenna Dome measurements.

2

Program of requirements

As stated earlier, the goal of this thesis is to provide a design procedure to characterize a beam-forming system and design an error model for the system. During the design process, a few requirements were set and several choices and assumptions were made, all of which are listed below.

Requirements

- The BBoxOne 5G 28GHz [2] is the beamforming system that will be modelled and characterized.
- The operation frequency range is from 24GHz to 30GHz.
- Monte Carlo [3] simulations will be used to verify the models.
- The final error model must be verified for a few beam patterns.
- The accuracy of the statistical models must be at least 99.7%.

Choices

- 50MHz measurement resolution, 121 frequency points within operating frequency.
- IF bandwidth of PNA is 300 Hz for more accurate data.
- The Law of large numbers [4] suggest that the deviation of all samples decreases with the number of samples, $\sigma/\sqrt{n}$. 30 measurement were therefore chosen to find the mean.
- 5° phase step and 0.5 dB gain step [2].
- RF power sources are set to -10 dBm.
- The maximum deviation of the standard model is 3σ, covering $1 - 2\Phi(-3) \approx 99.7\%$ [5, pp. 129] of all possible outcomes.

Assumptions

- Assume measurement noise is white Gaussian noise.
- Assume coupling between patch antenna's is negligible.
- Assume that the influence of external sources, like temperature change, has no major impact on the measurements.
- Assume that the direct transfer and leakage effect are independent for both gain and phase output of the beam-forming system.

3

Measurement setup

In order to characterize the beam-forming system, S-parameter data will be measured using a network analyzer. Multiple measurements for different system settings will be carried out using this setup. The measurement setup used in this project can be seen in figure 3.1 and consist of the components listed below. The computer uses MATLAB and code published by TMYTEK [6] to retrieve the measurement data from the PNA and control the BBox via LAN [7].

- BBoxOne 5G 28GHz [2] (beam-forming system)
- E8361A PNA Network Analyzer [8]
- 3,5mm SMA coaxial cables
- SMA to mini SMP adapter
- Cable support
- PC with MATLAB and code from TMYTEK [6]

3.1. PNA calibration

Before measuring the beam-forming system with the PNA, the test setup has to be calibrated. The setup is calibrated with the SMA cables connected using a calibration kit to remove unwanted errors introduced throughout the test setup. The Rosenberger RPC-3.50 Calibration Kit model 03CK10A-150 was used. Calibrating the PNA is crucial for obtaining accurate S-parameter measurements of the beam-forming system. The measured data for an uncalibrated PNA will contain data related to the system, but also data from other factors, such as internal fluctuations of the PNA and cable attenuation. This is not desired since the beam-forming system characteristics should be independent of the setup,

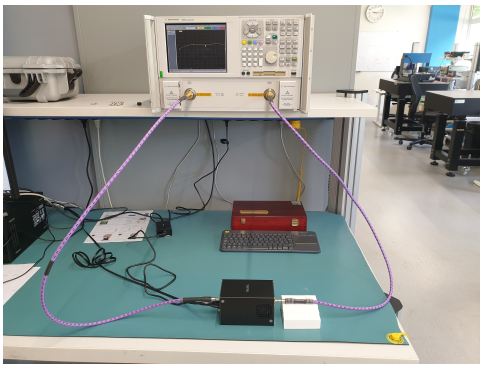

(a) Beam-forming system measurement setup

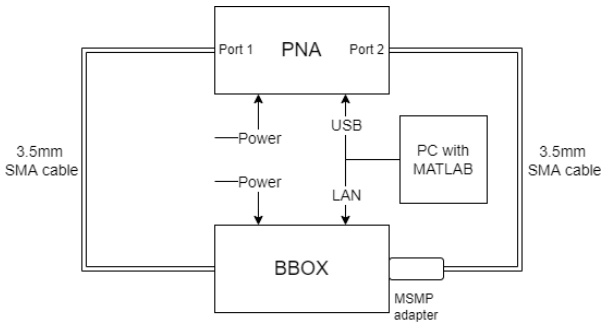

(b) Schematic of measurement setup

Figure 3.1: S-parameter measurement setup

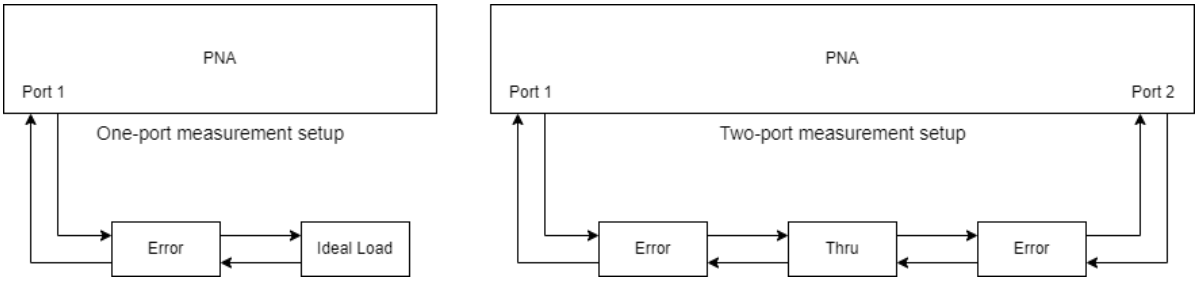

Figure 3.2: One-port and two-port measurement setups

and the system will eventually be used in different setups with different equipment.

Figure 3.2 shows a simple one-port and two-port measurement setup with error models modeling the PNA internal fluctuations and cable attenuation. In an ideal measurement setup, the measured return loss of the one-port setup is a flat response at $-\infty$ dB and the thru measured of the two-port setup is also a flat response at 0 dB. But this is not the case in a real, non-ideal, setup as seen in figure 3.3.

The PNA is therefore calibrated with a calibration procedure known as SOLT, Short-Open-Load-Thru, [9] with an unknown Thru [10]. This is a common technique and calibration kits with these standards are readily available. The calibration is done such that the error models in figure 3.2 are (mostly) compensated as seen in figure 3.4. It can be seen that the calibration is acceptable but not perfect.

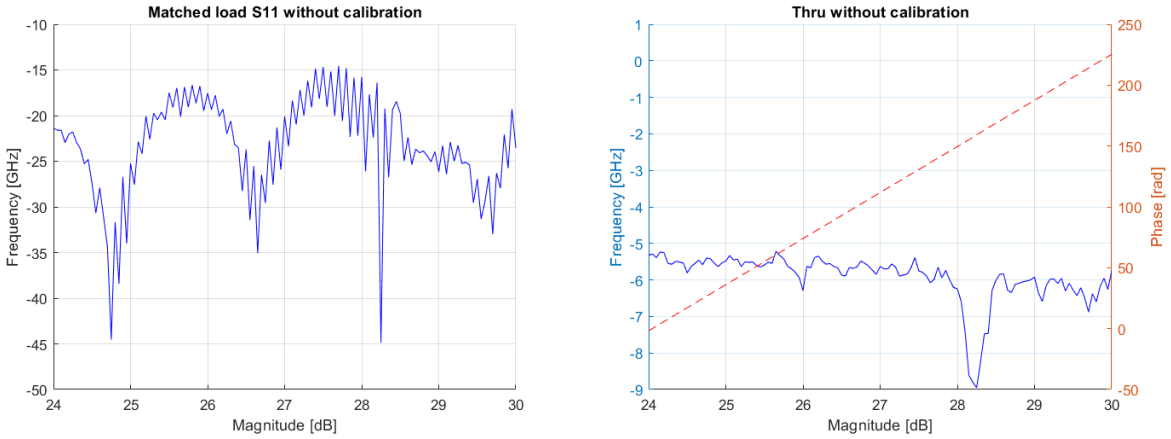

(a) Return loss without calibration

(b) Thru without calibration

Figure 3.3: Measurements without calibration

3.2. Thru compensation

As mentioned before, calibrating the setup cannot fully remove all unwanted behaviours from the measurement data as seen in figure 3.4. The data acquired from the PNA still needs to be digitally processed to remove the data error caused by the calibration. In the case of the beam-forming system, only the S21 parameter measurements had to be compensated. First, several thru measureents were performed after calibration. The average was then used to compensate the beam-forming system measurements. Both the compensation data and the system measurements were split into two parts, magnitude and phase part. The compensation for each frequency point of each part was done according to equations 3.1 and 3.2. Of course, every time the setup is re-calibrated, new thru measurements have to be made for the compensation.

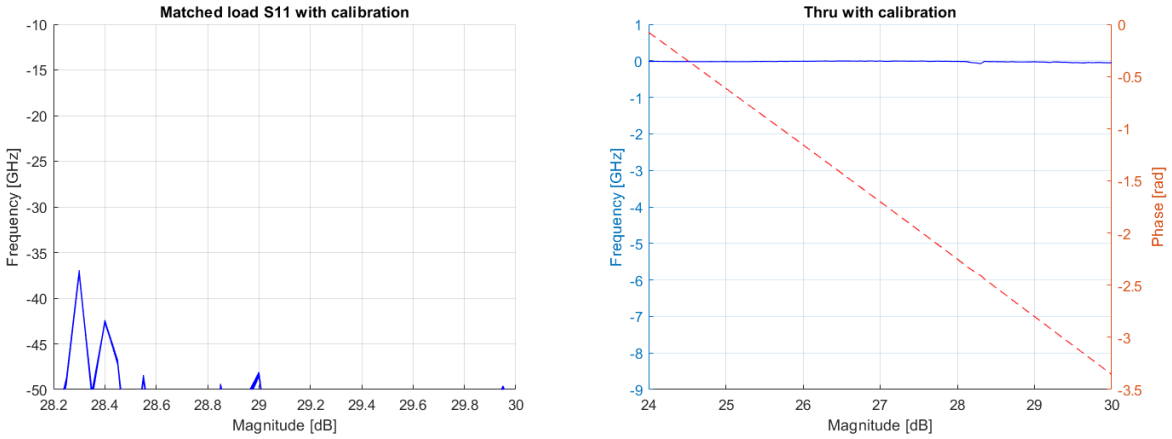

(a) Return loss with calibration

(b) Thru with calibration

Figure 3.4: Measurements with calibration

$$|S21_{system}| = |S21_{measured}|/|S21_{thru}| \tag{3.1}$$

$$\angle S21_{system} = \angle S21_{measured} - \angle S21_{thru} \tag{3.2}$$

4

SD and statistical model

The beam-forming system can be split into two parts, the channel control and the antenna array. The channel control part controls the output gain and phase of each channel of the beam-forming system within the operating bandwidth and a range of gain and phase settings. The antenna array part consist of 16 coaxially fed patch antenna's transmitting the output signals of all channels. This chapter discusses the design process of a model for the channel control part for the error model.

4.1. SD model

The channel control model models the part of the BBox One 5G 28GHz that provides additional gain and phase to a RF input signal per channel. To do this, a number of different system behaviors had to be analyzed and were first modelled as standard deviation models. These behaviors are:

- The frequency dependency of the output with fixed gain/phase settings as a base model.
- The direct transfer of the gain/phase setting.
- Leakage behaviour of the gain/phase setting.
- The power leakage from one channel to another.

4.1.1. Base model

The first step taken to create the channel control model was to establish a base model for the gain and phase behavior for all channels. The base model simply models the system's behaviour over the entire operating bandwidth with fixed gain and phase settings. The data used to create the base model consist of 30 measurements of each channel with -6 dB gain and 0° phase. From figure 4.1 it can be seen that all channel measurements are very similar with different horizontal and vertical offsets. Creating a model from this will result in a large maximum deviation which is not desired. Therefore, an array of offset values was included, an offset for each channel, to minimize the maximum deviation. These offset values can be found in table 4.2.

After applying the offset, the average of the data was taken and a curve fit model was created, which can be seen in figures 4.2 and 4.3. The figures show the base gain and phase model with the optimized data and the error between model and data. The gain model was chosen, as the best fit, to be a sum of five sinuses with the coefficients from table 4.1. The phase model was chosen to be a second order polynomial function as the best fit. The error of a first order polynomial is too large and higher orders are over fitting the data.

$$\text{Base magnitude model} = -0.2494 + \sum_{i=1}^{5} a_i \sin(b_i f + c_i) \text{ dB} \quad , \quad 0.9681 \text{ dB max deviation} \tag{4.1}$$

$$\text{Base phase model} = 0.09503 \cdot f^2 - 13.01 \cdot f + 255.7184 \text{ rad} \quad , \quad 0.3487 \text{ rad max deviation} \tag{4.2}$$

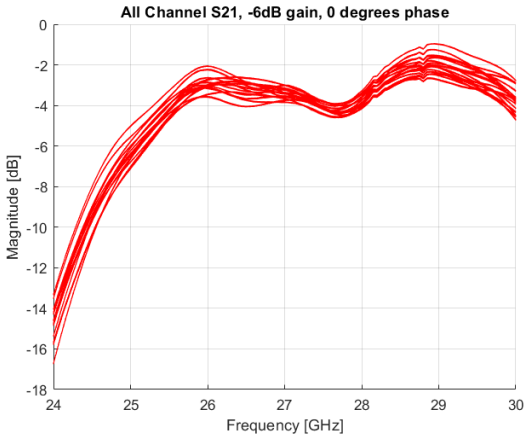

Figure 4.1: Raw measurement data from all channels with -6 dB gain and 0° phase

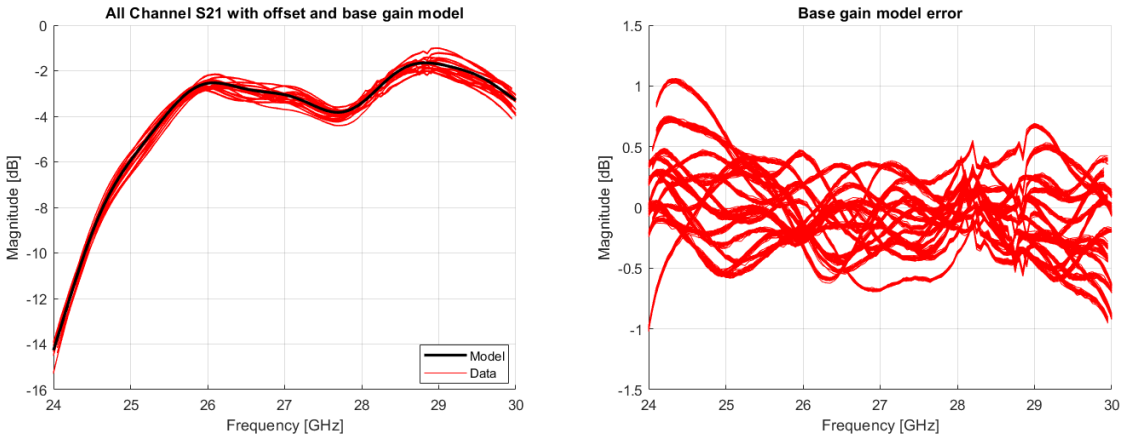

(a) Measurement data with offsets and base magnitude model curve

(b) Base magnitude model error with respect to data

Figure 4.2: Raw base magnitude model data with offset and curve fitted model

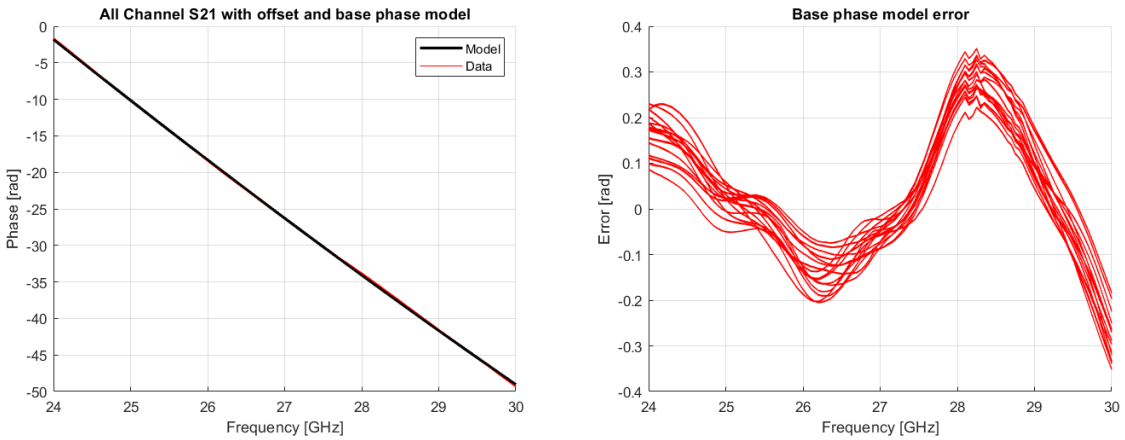

(a) Measurement data with offsets and base phase model curve

(b) Base phase model error with respect to data

Figure 4.3: Raw base phase model data with offset and curve fitted model

4.1.2. Direct transfer

The direct transfer models model the direct relation between the gain/phase setting of the BBox and the measured relative gain/phase. The gain at -6 dB and the phase at 0° were here chosen as the

Table 4.1: Base gain model coefficients

i	a	b	c
1	24.92	0.1139	9.268
2	5.308	0.8156	5.475
3	1.904	1.736	8.094
4	0.6627	2.46	17.55
5	0.1989	4.829	-16.52

Table 4.2: Channel offset coefficients for base both base models

	Gain model		Phase model
Channel	Horizontal offset [MHz]	Vertical offset [dB]	Vertical offset [dB]
1	0	0	0
2	50	-0.4189	-0.1614
3	50	-0.2431	-0.0575
4	-50	-0.1159	0.1314
5	50	-0.4241	-0.0020
6	50	-0.1057	-0.0607
7	50	0.4674	-0.0457
8	-50	-0.2204	0.0725
9	-100	-0.1426	0.0165
10	-50	-0.7318	-0.0063
11	-50	-0.4517	-0.1067
12	-50	-0.6559	0.5868
13	50	-0.3730	0.0848
14	100	-0.5507	-0.0057
15	100	-0.0809	-0.1439
16	-50	-0.1458	0.1217

reference. It was assumed that both direct relations do not cause any drastic changes to each other. In other words, the direct transfer model of the gain does not show any noticeable changes at different phase settings, and the direct transfer model of the phase does not show any noticeable changes at different gain settings.

Figures 4.4 and 4.5 show the direct transfer models. It can be seen that the relations are linear. A linear model was therefore chosen as seen in equations 4.3 and 4.4. Here, $G_{applied}$ and $P_{applied}$ are the applied gain and phase respectively. In figure 4.5b it can be seen that the error follows a certain pattern. This is due to the fact that the phase of the BBox is increased in steps, which means the error to the model increases when the phase goes to the next step, and decreases again until the next step is taken.

$$\text{Gain model} = 1.005 \cdot G_{applied} + 5.9922 \text{ dB} \quad , \quad 1.0149 \text{ dB max deviation} \tag{4.3}$$

$$\text{Phase model} = 0.0174 \cdot P_{applied} - 0.0904 \text{ rad} \quad , \quad 0.2003 \text{ rad max deviation} \tag{4.4}$$

4.1.3. Gain and phase correlation

Besides the direct relation between gain/phase setting and output gain/phase, there is also an unwanted correlation behavior where the gain setting causes fluctuations in the output phase. The same for the phase setting and the output gain. This correlation behavior can be seen in figures 4.6 and 4.7 with their respective model from 4.6 and 4.6.

$$\begin{aligned}\text{Phase leakage} = {} & 0.2662 \sin(0.01943 P_{applied} + 2.659) + \\ & 0.1787 \sin(0.007615 P_{applied} - 2.226) - 0.0188 \text{ dB} \quad , \quad 0.7313 \text{ dB max deviation}\end{aligned} \tag{4.5}$$

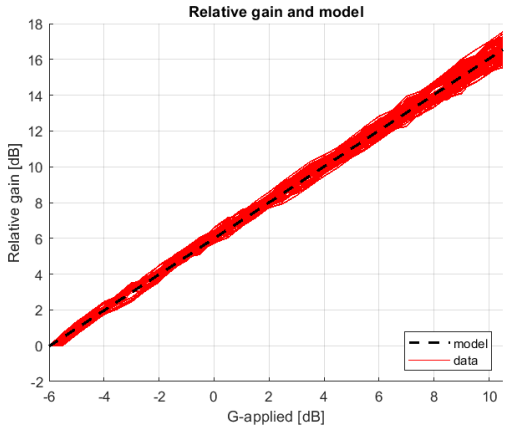

(a) Direct gain model and raw data

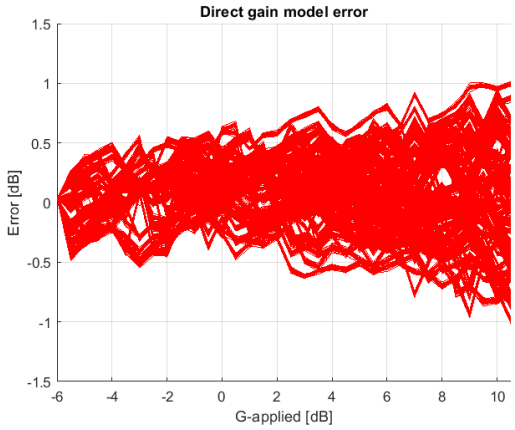

(b) Direct gain model error

Figure 4.4: Direct gain model

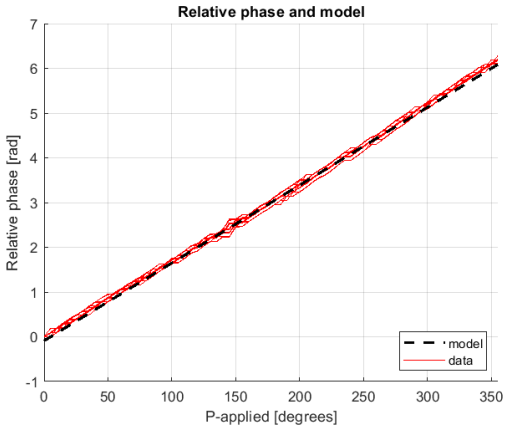

(a) Direct phase model and raw data

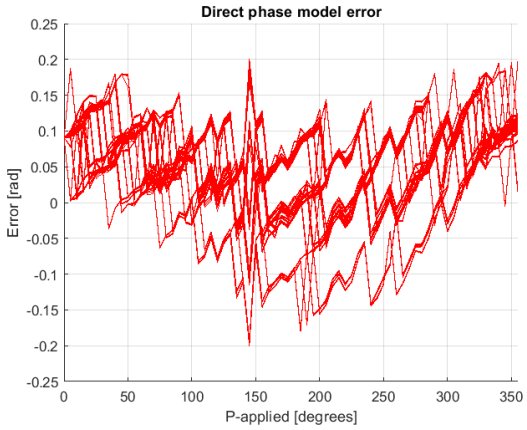

(b) Direct phase model error

Figure 4.5: Direct phase model

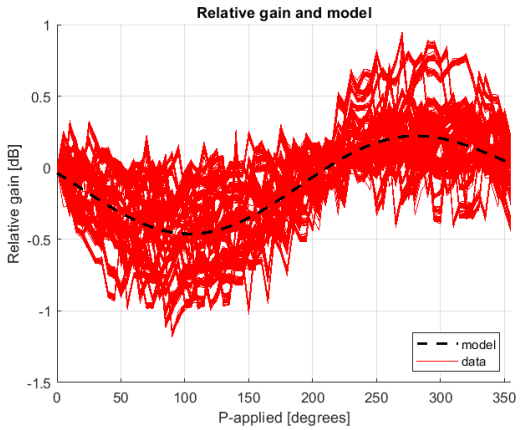

(a) Phase leakage model and raw data

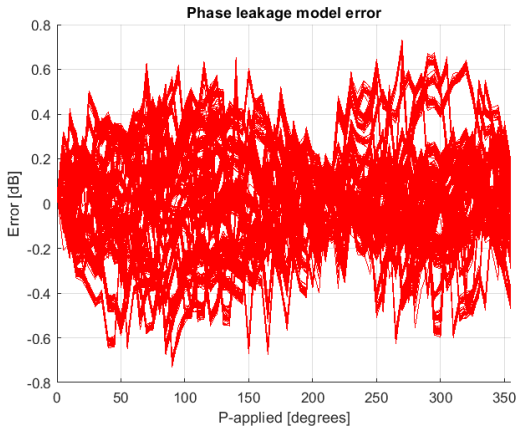

(b) Phase leakage model error

Figure 4.6: Phase leakage model

$$\text{Gain leakage} = -0.0003913G_{applied}^2 + 0.003895G_{applied} + 0.0598 \text{ rad} \quad , \quad 0.1978 \text{ rad max deviation} \tag{4.6}$$

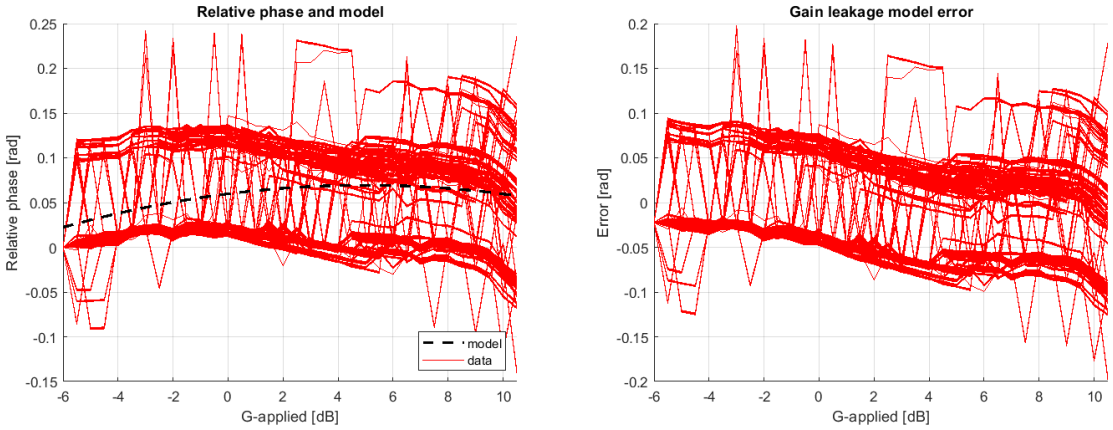

(a) Gain leakage model and raw data

(b) Gain leakage model error

Figure 4.7: Gain leakage model

4.1.4. Channel leakage

The beam-forming system is not a completely ideal system. When one of the channels is on and transmitting, its signal will leak into the other channels and cause interference. This is evident by figure 4.8 were it is shown that other channels, beside channel 1, can have their output leaked into channel 1. The measurements were conducted by measuring the output signal at channel 1 with channel 1 turned off. The other channels were turned on one by one and had a $50\ \Omega$ load attached to them. Since the leakage is not sufficiently large, it can be neglected and it will not be included into the channel control model. Leakage measurements of all channels can be found in appendix A.

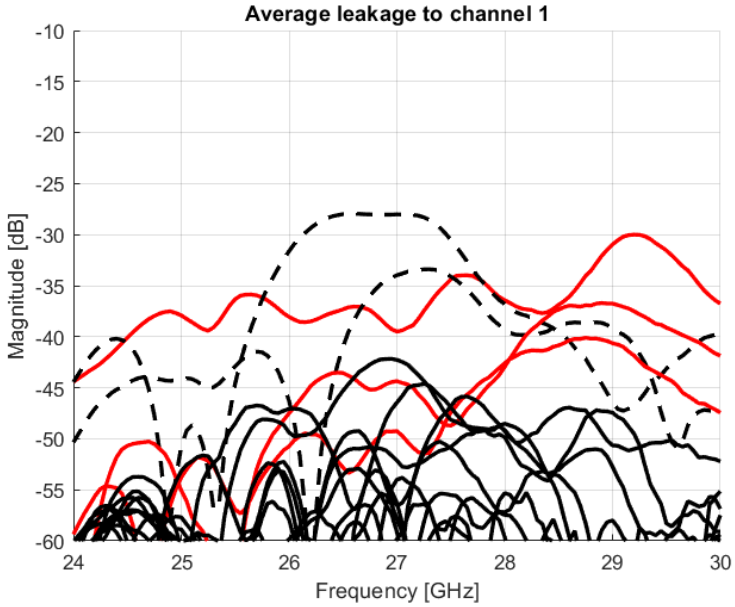

Figure 4.8: Average leakage to channel 1

In figure 4.8 it can be seen that there are three types of data indicated by the color of the line and whether the line is dotted or not. The different data types indicate whether the leakage came from a 'nearby' channel, a 'far away' channel or a 'far away' channel on the same board as the channel under measurement. The list below indicates which data types in the figure belongs to which channel and figure 4.9 provides a visual aid to clarify the measurements. Each channel is indicated by a circle with a number below it and each row of channel correspond to a single board. The colors in the figure

correspond to the colors in the measurement data.

- Solid red: nearby channel
- Dotted black: far away channel on the same board
- Solid black: far away channel

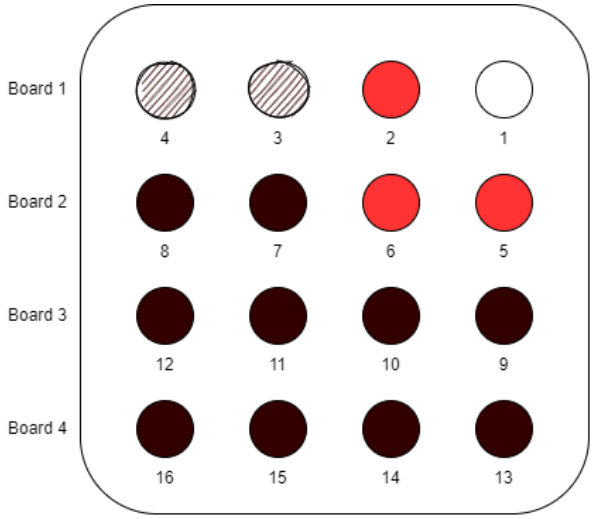

Figure 4.9: Data type indicator for measurement form figure 4.8

4.1.5. Complete model

The complete channel control model consist of all models described in the previous subsections. The behaviors of each channel on the beam-forming system can then be simulated. To simulate the behavior of a channel, the base model, with different offsets per channel, the direct transfer models and leakage models are used to estimate the output of a channel. Additional uncertainties from the maximum deviations of each model are also added. It is assumed that uncertainties are normally distributed with zero mean and the maximum deviation of the models being 3σ, 99.7% of all data possibilities are within maximum deviation boundary. Table 4.3 contains a collection of all models used for the channel control model.

4.2. Statistical model

The standard deviation model contains three normally distributed noise variables. These variables cause the model to deviate from its original design. Using Monte Carlo simulations [3], a statistical model of the standard deviation model was created and the boundaries of the standard deviation model were then also found. These boundaries were later used to verify and validate the standard deviation model. Figure 4.10 shows an example of a Monte Carlo simulation with 10^4 iterations for the channel control model.

Table 4.3: Model equations and maximum deviation

Model name	Equation	Max deviation
Base magnitude	$-0.2494 + \sum_{i=1}^{5} a_i \sin(b_i f + c_i)$ *see table 4.1 for coefficients*	0.9681 dB
Direct gain	$1.005 \cdot G_{applied} + 5.9922$	1.0149 dB
Phase leakage	$0.2662 \sin(0.01943 \cdot P_{applied} + 2.659) + 0.1787 \sin(0.007615 \cdot P_{applied} - 2.226) - 0.0188$	0.7501 dB
Base phase	$0.09503 \cdot f^2 - 13.01 \cdot f + 255.7184$	0.3487 rad
Direct phase	$0.0174 \cdot P_{applied} - 0.0904$	0.2083 rad
Gain leakage	$-0.0003913 \cdot G_{applied}^2 + 0.003895 \cdot G_{applied} + 0.0598$	0.2573 rad

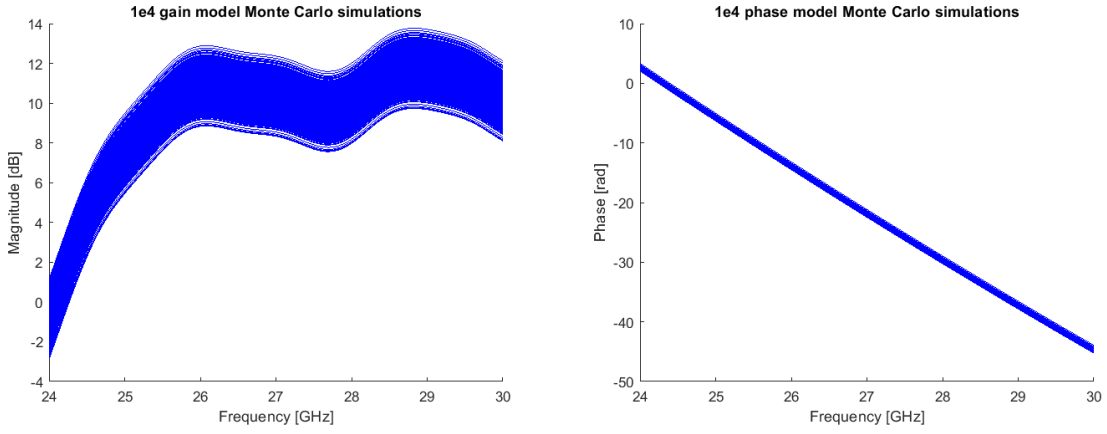

(a) Gain model **(b)** Phase model

Figure 4.10: Example of Monte Carlo simulations with channel control model to find boundaries

5

Antenna characteristics

To complete the error model of the beam-forming system, a model will be developed of the provided antenna array. This model simulates the radiation pattern created by the antenna array with the excitation provided by the channel control part. The design process of the antenna array model was split into multiple steps. First, near field (NF) radiation pattern data was collected of a single antenna patch. The near field pattern is then transformed to a far field (FF) radiation pattern. With this, an array factor is created to complete the radiation pattern of the beam-forming system. By measuring a single element and knowing the array factor, the radiation pattern of the total array can be found, as shown in 5.1. As stated earlier, it was assumed that the coupling between antenna's could be neglected.

$$\text{Single element} \times \text{Array factor} = \text{Array total} \tag{5.1}$$

5.1. Measurement setup

In order to measure the near field pattern of an antenna patch, a near field measurement setup is used. The near field measurement setup in figure 5.1 can perform planar scanning by moving the CNC machine around and stopping at specific intervals to measure near field data from the BBox antenna's. The list of components of the near field measurement setup can be found below.

- Computer numerical control (CNC) machine
- PNA
- 3,5mm SMA coaxial cables
- Open waveguide with low gain
- BBoxOne 5G 28GHz
- Computer with MATLAB
- Absorption material

5.2. Sampling

There are many ways to perform planar scanning. Some examples are plane-rectangular, plane-polar and bipolar [11]. In the case for near field measurements of the BBox antenna's, plane-rectangular scanning was chosen as the scanning technique due to its simplicity. The space near a radiating antenna can be divided into three sections, reactive near field, radiating near field and far field. The radiating near field is the region of interest when acquiring data about the near field. This region spans an area with a specific radius dependent on the antenna dimensions and the transmit frequency of the antenna. 5.2 shows the relation between near field distance (NFD), the wavelength and the dintance D, which is the largest distance within the antenna array. Furthermore, for proper sampling, the spacing between sample positions must also fulfill the criteria $\Delta d \leq \lambda/2$ from sampling theorem. A spacing of approximately $\lambda/8 \approx 0.1$mm was chosen to have a sufficiently accurate measurement for the NF.

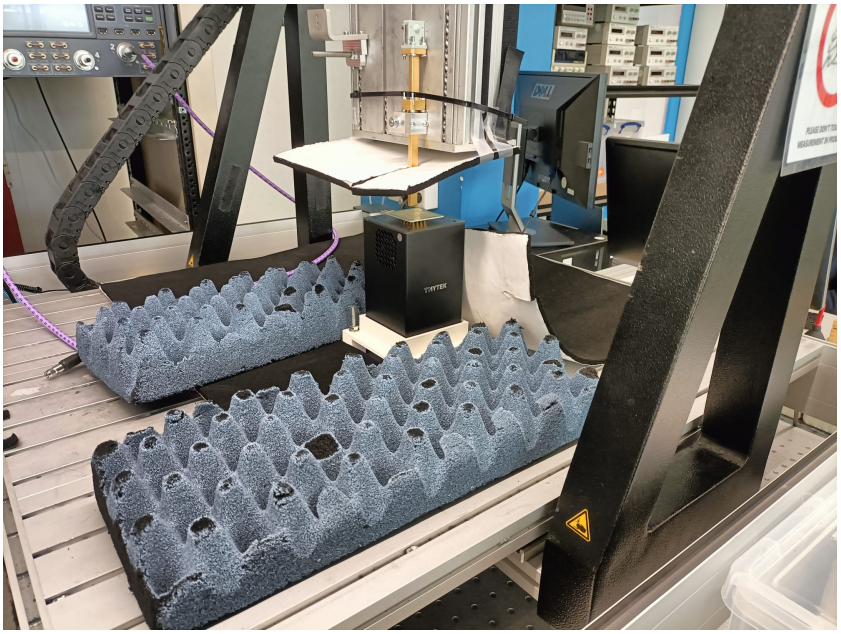

Figure 5.1: Near field measurement setup

$$NFD = 0.62 * \sqrt{D^3/\lambda} \tag{5.2}$$

The area scanned was determined by moving the CNC machine up to a point where the measured S21 parameter would be below 20 dB. This distance was doubled and taken as the side of the square area to be scanned, which in this case was a square of 12cm$\times$12cm. First the area was was centered and scanned around a single active antenna element. After this, the area was centered and scanned for the full active antenna array.

5.3. Time-Gating

Due to the imperfect measurement setup, many reflections of the to be measured radiation pattern are also included into the measurements. The technique called Time-Gating [12, 13] was chosen to filter as many reflections out of the measurement data. This is done through the principle shown in figure 5.2 where the spectrum data is first transformed to the time domain via inverse Fourier transform (ifft) [14]. Within the time domain data, the data related to the direct path radiation is located and isolated from the 'noise'. The time-gated data is then transformed back using a Fourier transform to obtain the spectrum of the direct path radiation. An example is shown in figure 5.3.

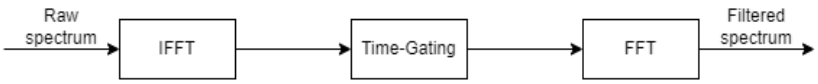

Figure 5.2: Time-Gating principle

5.4. NF to FF transform

The near field measurements by themselves are not useful. The Antenna Dome measures the radiation in the far field region of the antenna's. The obtained NF measurements from time-gating were therefore transformed to far field data with a NF to FF transformation. The transformation of the measured near field data was done with the plane wave expansion using Fourier transform technique [15] with the formula below. The far field electric field were then determined by 5.6. With 5.7, the directivity of the far field pattern was determined. It should be noted that the $1/4pi^2$ term in 5.3 and the $j\frac{ke^{-jkr}}{2\pi r}$ term in 5.4 and 5.5 are missing. This is because E^2_{abs} was normalized for the model which simplified

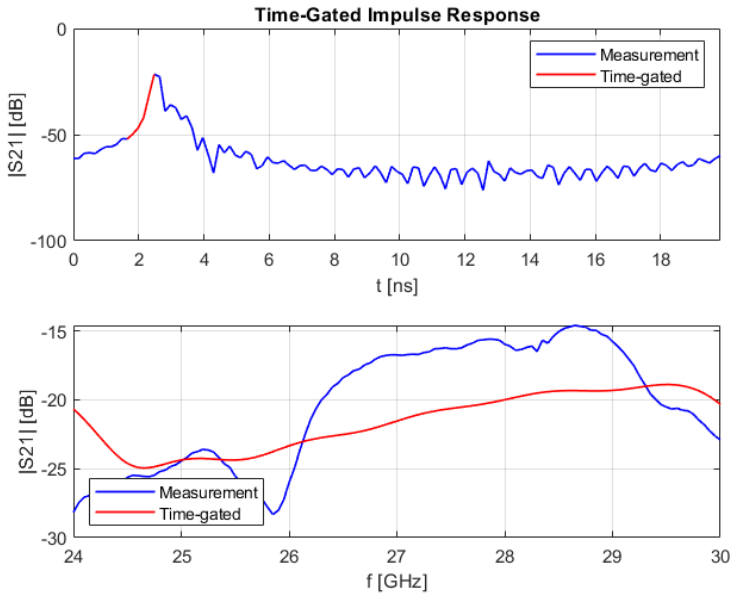

Figure 5.3: Example of implementing Time-Gating

the formula's.

$$f(k_x, k_y) = \int_{-\infty}^{\infty} \int_{-\infty}^{\infty} E(x, y) e^{-j(k_x x + k_y y)} dx dy \tag{5.3}$$

$$E_\theta(\phi) = f(k_x, k_y) sin(\phi) \tag{5.4}$$

$$E_\phi(\theta, \phi) = f(k_x, k_y) cos(\theta) cos(\phi) \tag{5.5}$$

$$E_{abs}^2 = E_\theta^2 + E_\phi^2 \tag{5.6}$$

$$D = \frac{4\pi E_{abs}^2}{P_r ad} \tag{5.7}$$

5.5. Array factor

The array factor (AF) [16, 17] is a function showing the effect of an antenna array. When the AF is multiplied with the radiation pattern of a single antenna element in the array, then the radiation pattern of the entire antenna array can be determined. The AF expression for a 4×4 2D uniformly spaced antenna array can be seen in 5.8 [18] and in the code in B. This expression is then normalized using 5.9 before using it to determine the far field radiation pattern.

$$AF_{eq}(u, v) = \sum_{m=0}^{3} \sum_{n=0}^{3} I_{mn} e^{jk(md_x(u-u_0)+nd_y(v-v_0))} \tag{5.8}$$

Here $u = \sin\theta \cos\phi$ and $v = \sin\theta \sin\phi$ indicate the observation angles when the main beam is looking into the direction of u_0 and v_0. m and n indicate the one antenna within the array with weight I_{mn}. d_x and d_y indicate the distance between two antenna's and are the same because the array is uniformly spaced.

$$AF(u, v) = \frac{AF_{eq}(u, v)}{|AF_{eq,max}|} \tag{5.9}$$

5.5.1. Uniform weights

As seen in the expression for the array factor with an 2D uniform spaced antenna array, there is a weight term I_{mn}. By applying different weights to each antenna, different radiation patterns can be

realized. The simplest option is to provide uniform weights for all and radiate Broadside [19]. Figure 5.4 shows the broadside AF of a 4 by 4 antenna array.

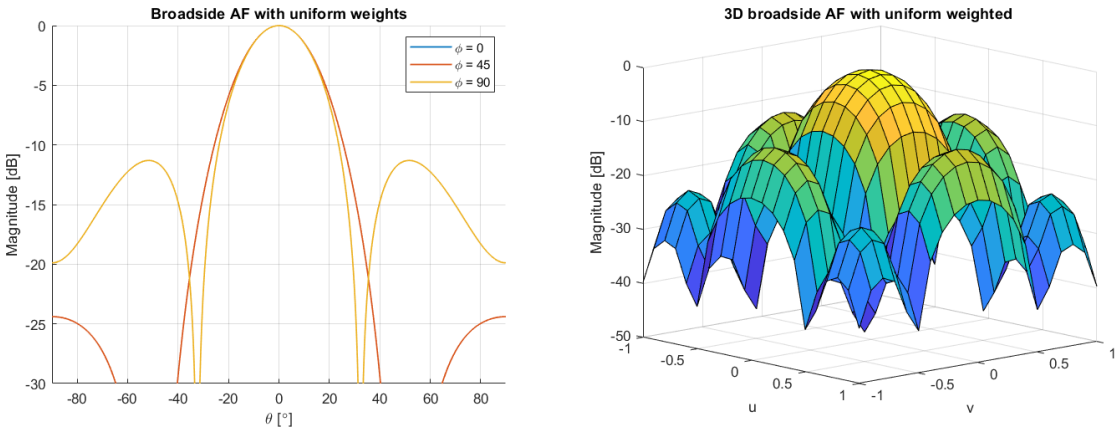

(a) Broadside AF with uniform weights at different angles

(b) 3D plot of broadside AF with uniform weights

Figure 5.4: Broadside AF at different main beam angles

5.5.2. Dolph-Chebyshev

Besides uniform weights, non-uniform weights are also an option. One special way to implement non-uniform weight distribution is the Dolph-Chebyshev weight distribution [20] where weights are chosen such that the magnitude of the side-lobes can be controlled. Lowering the side-lobes has the advantage of stopping energy leakage into unwanted directions, but comes at the cost of a wider main lobe. The array factor for an even number of elements using the Dolph-Chebyshev method is given by:

$$(AF)_{2M} = \sum_{n=1}^{M} a_n cos[(2n-1)u] \tag{5.10}$$

where

$$u = \frac{\pi d}{\lambda} cos(\theta) \tag{5.11}$$

In the case of the BBox, $\frac{d}{\lambda} = \frac{1}{2}$, and thus 5.11 simplifies to $u = \frac{\pi}{2} cos(\theta)$. The BBox has an 4×4 array, which means that M=2, and only two cosine elements need to be calculated. Using the trigonometric identities below, the weights for a 1-dimensional linear array can be obtained from 5.12 [21].

$$\begin{aligned} m = 1 \qquad & cos(mu) = cos(u) \\ m = 2 \qquad & cos(mu) = cos(2u) = 2cos^2(u) - 1 \\ m = 3 \qquad & cos(mu) = cos(3u) = 4cos^3(u) - 3cos(u) \end{aligned}$$

$$AF_4 = a_1 cos(u) + a_2 cos(3u) = a_1 cos(u) + a_2[4cos^3(u) - 3cos(u)] \tag{5.12}$$

These weights for a 1-dimensional linear array can then be weighted with the same weights in the other dimension to obtain the 4×4, 2-dimensional Dolph-Chebyshev weights, as shown in figure 5.5. The resulting array factor can be seen in figure 5.6.

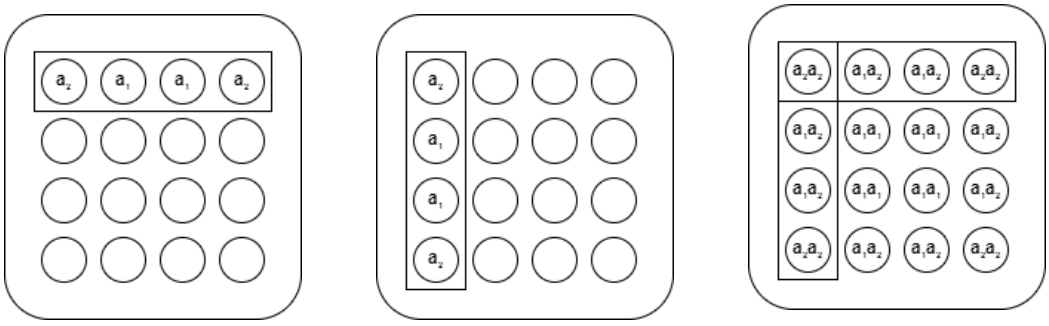

(a) Horizontal array weights

(b) Vertical array weights

(c) Complete array Dolph-Chebyshev weights

Figure 5.5: Computation of the Dolph-Chebyshev weights

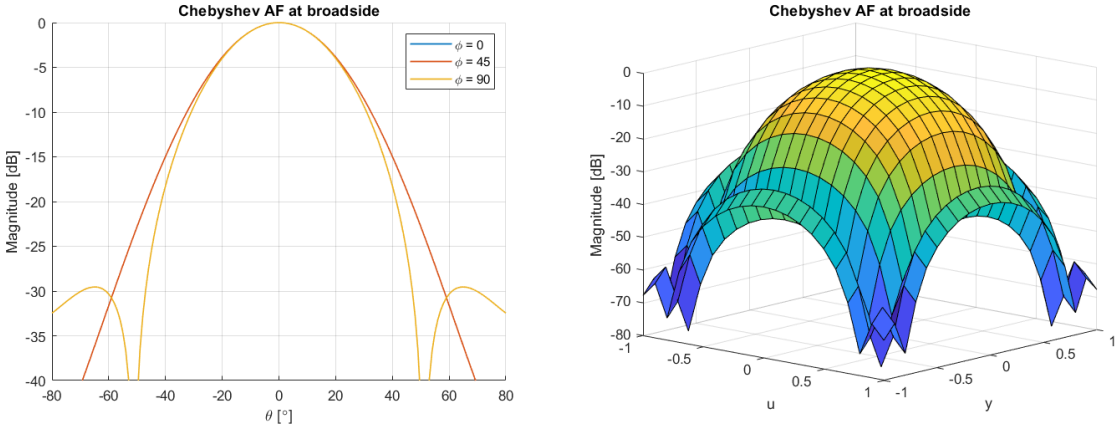

(a) Chebyshev AF at different angles

(b) 3D plot of chebyshev AF

Figure 5.6: Dolph-Chebyshev AF

6

Error model

The previous sections showed the procedures for designing the models for the channel control part and the radiation pattern of a 4×4 antenna array. To complete the error model of the whole beam-forming system, these two models have to be combined. This is done by using the output gain and phase of the channel control model as the excitation of the antenna array model. Monte Carlo simulations were again used to obtain the boundaries of the error model. The error model code can be found in B.

The final crucial step to designing the error model of the beam-forming system is to verify the created model. The verification was split into two parts, channel control and complete verification. The channel control verification was done through many random measurements for each channel 6.1 to verify the boundaries set by Monte Carlo simulations. Figure 6.2 show an example of the real data within the boundaries created by Monte Carlo simulations. Each random measurement uses a gain en phase which was randomly chosen from an uniformly distribution of possibilities.

6.1. Test setup

In order to test the developed error model, the beam-forming system was put inside the antenna dome 1.0 to measure the radiation pattern at different settings, as seen in figure 6.1. It should be noted that the antenna dome 1.0 is not a perfect system. It does not have isolation panels to stop external interference or reflected radiation inside the dome. This means that there are some uncertainties in the measured data. The results will be discussed in the next chapter.

6.2. Verification

Verifying the complete error model was done in a similar way but including the array factor and single antenna element pattern. The normalized far field pattern of the single element near field measurements can be seen in 6.3a with there respective directivity in figure 6.3b. Monte Carlo simulations were then performed for the complete error model and compared with real far field measurement data of the beam-forming system with the same settings. This is shown in figure 6.4 where can be seen that simulations and measured pattern are not fully overlapping. There seem to be more other factors involved in the real data which were not accounted for in the models.

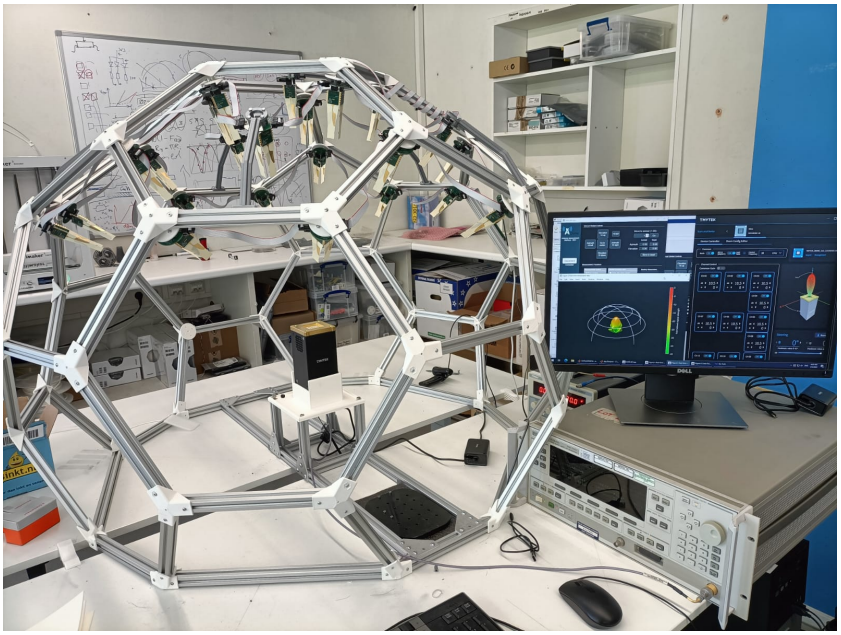

Figure 6.1: BBox beam pattern measurement setup using Antenna Dome 1.0

Table 6.1: Channel control model statistical test results using real data

Channel	Number of measurements within boundary	Number of measurements outside boundary	Success percentage [%]
1	58	2	96.7
2	58	2	96.7
3	56	4	93.3
4	58	2	96.7
5	58	2	96.7
6	58	2	96.7
7	59	1	98.3
8	60	0	100
9	60	0	100
10	59	1	98.3
11	57	3	95.0
12	58	2	96.7
13	60	0	100
14	59	1	98.3
15	59	1	98.3
16	59	1	98.3
All	936	24	97.5

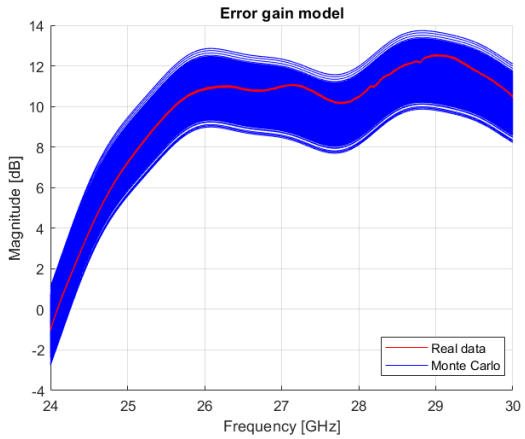

(a) Example of gain model verification

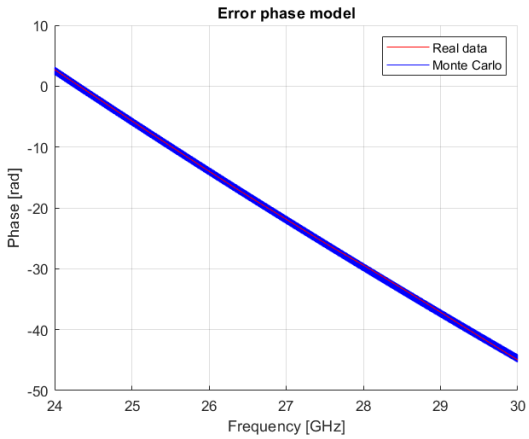

(b) Example of phase model verification

Figure 6.2: Example of channel control model verification

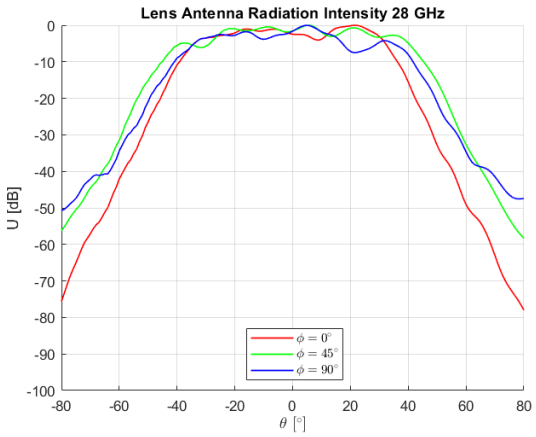

(a) Far field result of single patch antenna

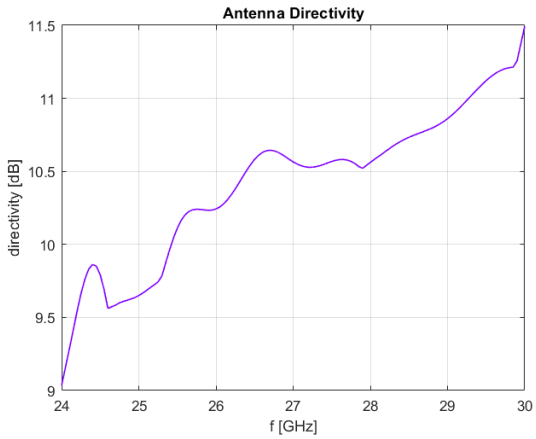

(b) Directivity of single patch antenna

Figure 6.3: Single antenna near field measurement results

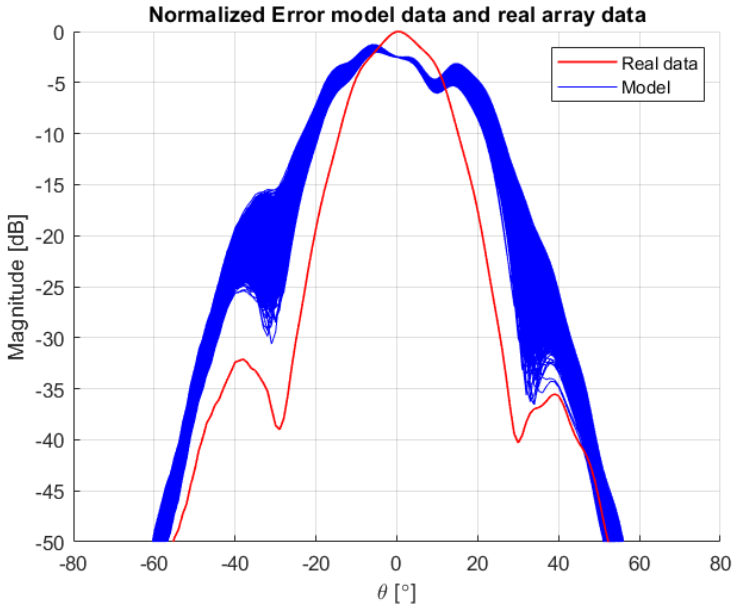

Figure 6.4: Error model simulation and real data

7

Conclusion

The purpose of this thesis is to show a design procedure for an error model of a beam-forming system. This error model is needed to calibrate and validate the functionality the Antenna Dome in order to test different antenna's with the dome. The BBox model was split into two main parts and a model was created for each part. The different models were created through curve fitting with real data and/or theoretical formula's. The models were put together to form the whole error model for the BBox and were verified with radiation pattern measurements. The results of the verification have shown that the channel control model is accurate enough to predict the behavior of the BBox. Unfortunately, the complete error model is not a good enough model to predict the far field radiation pattern of the BBox. This is mostly due to the antenna model and the deviation from the expected radiation patterns.

7.1. Future work

The designed error model is a reasonable model to predict the behavior of the BBox. But the design of the model is still build upon many assumptions. To improve the accuracy of the error model, further studies need to be conducted. The following improvements can be made.

- The study of the relationship between the direct transfer and the leakage behaviour of the BBox channels.
- Include probe correction to the near field measurements.
- Study the coupling effect between antenna patches.
- Improve near field measurements by including probe correction.

A

All channel leakages

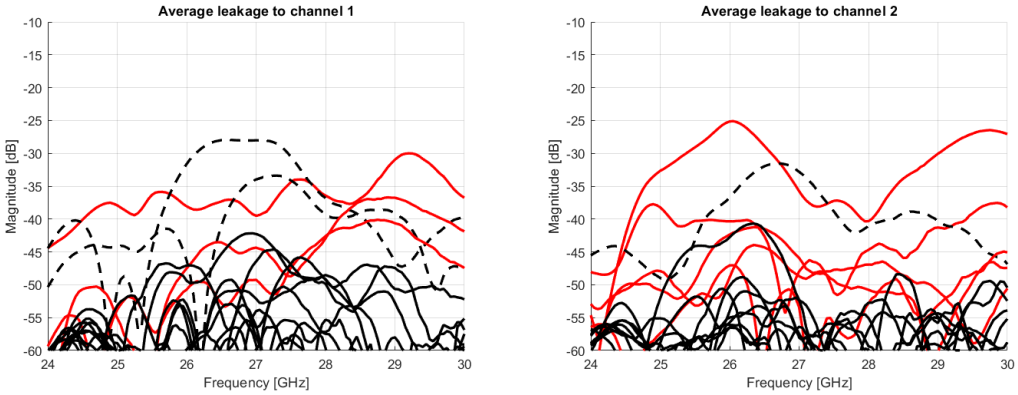

(a) Leakage to channel 1

(b) Leakage to channel 2

Figure A.1: Leakage measurement to channel 1&2

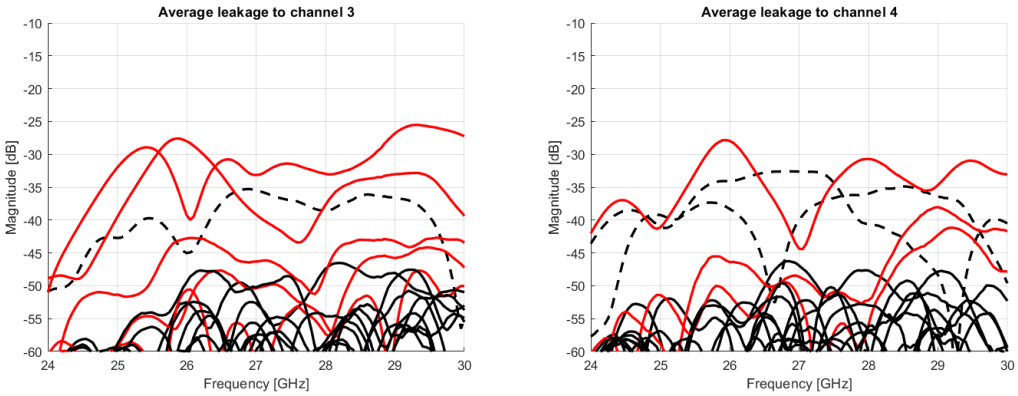

(a) Leakage to channel 3

(b) Leakage to channel 4

Figure A.2: Leakage measurement to channel 3&4

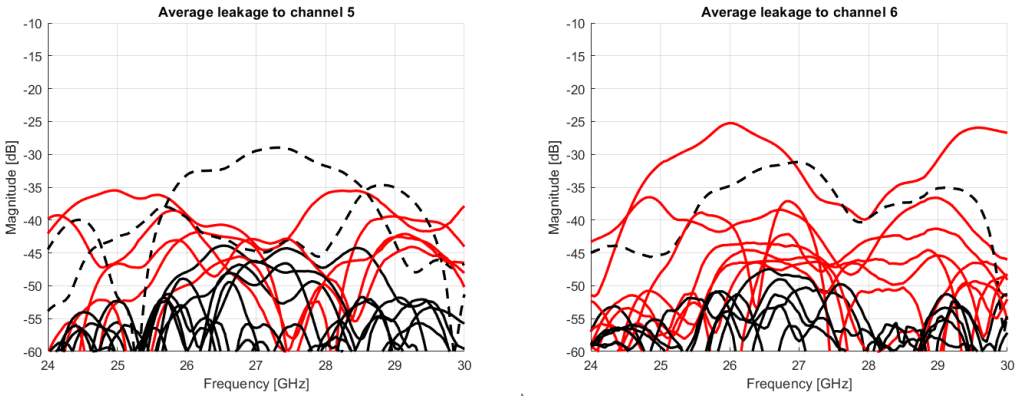

(a) Leakage to channel 5 **(b)** Leakage to channel 6

Figure A.3: Leakage measurement to channel 5&6

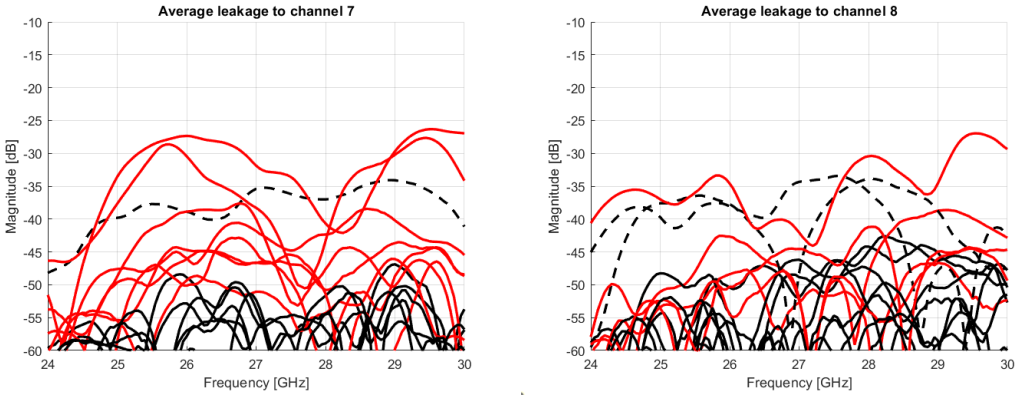

(a) Leakage to channel 7 **(b)** Leakage to channel 8

Figure A.4: Leakage measurement to channel 7&8

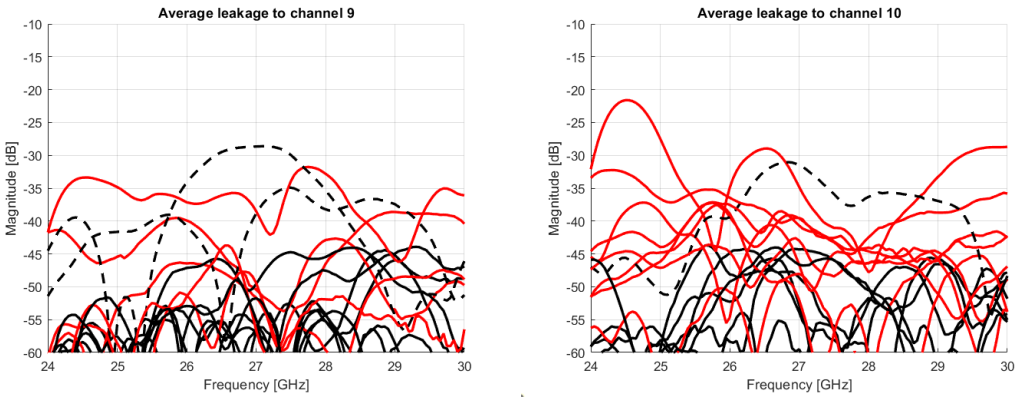

(a) Leakage to channel 9 **(b)** Leakage to channel 10

Figure A.5: Leakage measurement to channel 9&10

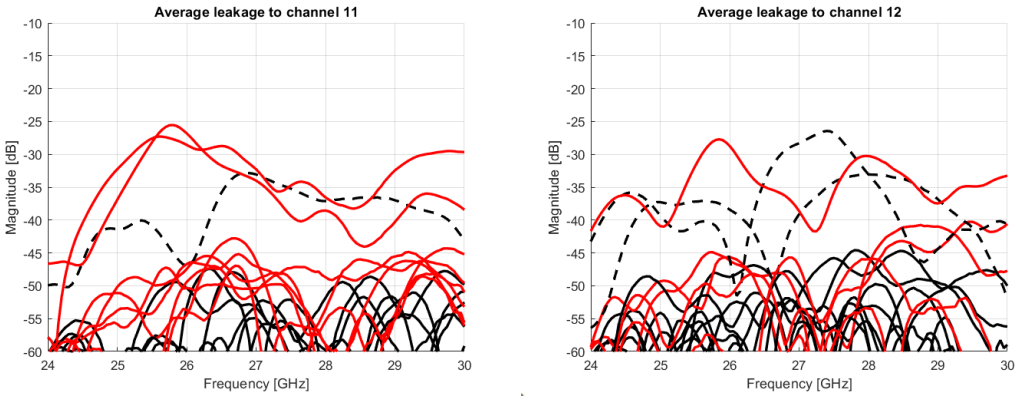

(a) Leakage to channel 11 **(b)** Leakage to channel 12

Figure A.6: Leakage measurement to channel 11&12

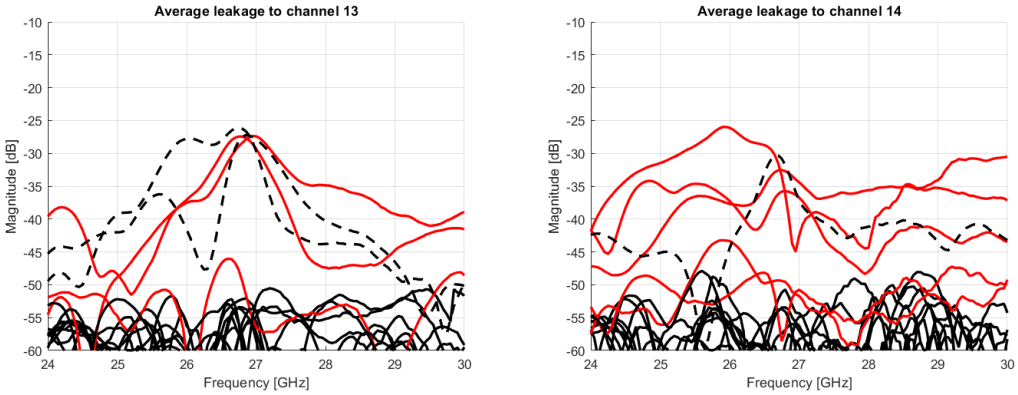

(a) Leakage to channel 13 **(b)** Leakage to channel 14

Figure A.7: Leakage measurement to channel 13&14

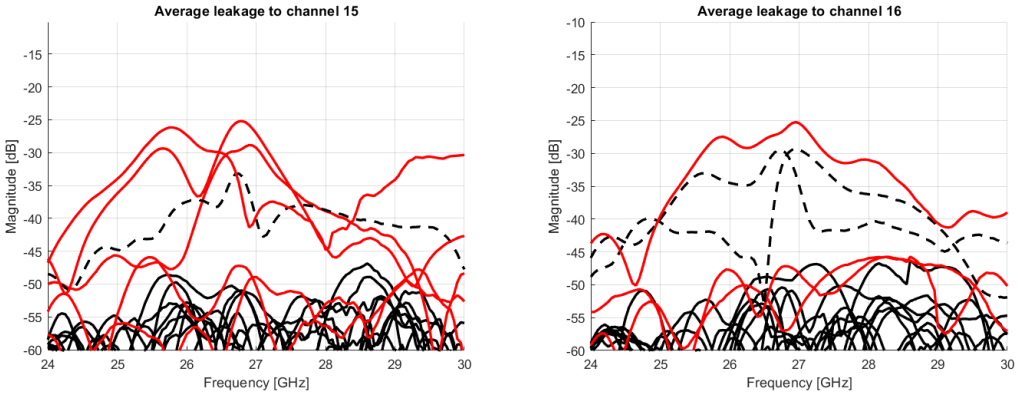

(a) Leakage to channel 15 **(b)** Leakage to channel 16

Figure A.8: Leakage measurement to channel 15&16

B

MATLAB code

B.1. SD model

```
function [MagModel, PhaseModel] = newSDmodel(CH,f,gain,phase)
    % TX model BBox One 5G with Standard deviation

    % Note:
    % Make sure that the measured data has been compensated due to VNA
    % internal errors (Thru compensation).

    % If phase model and measured phase do not overlap, then check the
    % difference. If difference is 2pi rad / 360 degrees, then there may be
    % a problem with the unwrap function.

    Nfreq = length(f);

    % List of max deviations (3 sigma)
    MagBaseDev = 0.9681; %dB
    MagGGDev = 1.0149; %dB
    MagPGDev = 0.7313; %dB
    PhaseBaseDev = 0.3487; %rad
    PhaseGPDev = 0.1978; %rad
    PhasePPDev = 0.2003; %rad

    % RNG deviation
    SDMagBase = normrnd(0,MagBaseDev/3,[1,1]);
    SDMagGG = normrnd(0,MagGGDev/3,[1,1]);
    SDMagPG = normrnd(0,MagPGDev/3,[1,1]);
    SDMagTotal = SDMagBase + SDMagGG + SDMagPG;
    SDPhaseBase = normrnd(0,PhaseBaseDev/3,[1,1]);
    SDPhaseGP = normrnd(0,PhaseGPDev/3,[1,1]);
    SDPhasePP = normrnd(0,PhasePPDev/3,[1,1]);
    SDPhaseTotal = SDPhaseBase + SDPhaseGP + SDPhasePP;

    %Checks
    if length(gain) > 1 || length(phase) > 1
        disp('gain and phase must be integer')
        return
    end

    % Base Magnitude
    % Base Magnitude model offsets
    % Horizontal offset table:
    offV = [0, -0.4189, -0.2431, -0.1159, -0.4241, -0.1057, 0.4674, -0.2204, -0.1426,
        -0.7318, -0.4517, -0.6559, -0.3730, -0.5507, -0.0809, -0.1458]; %dB
    % Vertical offset table (>0: move curve to the right ; <0: move curve to left):
    offH = [0,1,1,-1,1,1,1,-1,-2,-1,-1,-1,1,2,2,-1] * 0.05; %GHz
    %Coefficients
    a = [24.92  5.308   1.904   0.6627  0.1989];
    b = [0.1139 0.8156  1.736   2.46    4.829];
    c = [9.268  5.475   8.094   17.55   -16.52];
```

```
    FunMagBase = zeros(1,Nfreq) + offV(CH) - 0.2494;
    for ind = 1:length(a)
        FunMagBase = FunMagBase + a(ind)*sin(b(ind)*(f+offH(CH)) + c(ind));
    end


    % Gapplied to Mag
    p1 =       1.005;
    p2 =       6.083 - 0.0908;
    FunGG = p1*gain + p2;

    % Papplied to Mag
    a1 =      0.2662;
    b1 =     0.01943;
    c1 =       2.659;
    a2 =      0.1787;
    b2 =    0.007615;
    c2 =      -2.226;
    FunPG =  a1*sin(b1*phase+c1) + a2*sin(b2*phase+c2) - 0.0188;

    MagModel = FunMagBase + FunGG + FunPG + SDMagTotal;

    %--------------------------------------------------------------------------
    % Base Phase
    offsetV = [0, -0.1674, -0.0595, 0.1314, 0.4020, 0.6607, 0.3957, 0.3925, 0.2165, -0.0063,
        0.4067, 0.5868, 0.0848, -0.0057, -0.1439, 0.1217]; %rad
    p1 =     0.09503;
    p2 =      -13.01;
    p3 =       255.8 - 0.0816;
    FunPhaseBase = p1*(f.^2) + p2*f + p3 + offsetV(CH);


    % G-applied to Phase
    p1 =  -0.0003913;
    p2 =    0.003895;
    p3 =     0.04927 + 0.01053;
    FunGP = p1*gain.^2 + p2*gain + p3;

    % P-applied to Phase
    p1 =      0.0174;
    p2 =     -0.0334 - 0.0570;
    FunPP = p1*phase + p2;

    PhaseModel = FunPhaseBase + FunGP + FunPP + SDPhaseTotal;
end
```

B.2. Array factor

```
function [AFarr, AFmatrix] = BBoxAF(f, excite,theta,phi,theta0,phi0, plotindex)
%Returned AF values are complex
%Example: [temp1,temp2] = BBoxAF(28e9,ChebyshevweightsBBox,-80:80,[0 45 90],0,0,1);
c0 = 299792458;
k = 2*pi*f/c0;
d = 5e-3;

%Beam direction
u0 = sin(theta0*(pi/180))*cos(phi0*(pi/180));
v0 = sin(theta0*(pi/180))*sin(phi0*(pi/180));

%2D AF
AFarr = zeros(length(phi),length(theta));
for phiphi = 1:length(phi)
    u = sin(theta*(pi/180))*cos(phi(phiphi)*(pi/180));
    v = sin(theta*(pi/180))*sin(phi(phiphi)*(pi/180));
    for x = 0:(size(excite,2) - 1) %ch
        for y = 0:(size(excite,1) - 1) %brd
            AFarr(phiphi,:) = AFarr(phiphi,:) + (excite(y+1,x+1))*exp(1i*k*((x)*d*(u-u0) + y*
                d*(v-v0)));
        end
    end
```

```
end
if plotindex
    figure
    hold on
    grid on
    str = [""];
    for phiphi = 1:length(phi)
        temp = ['phi = ' num2str(phi(phiphi))];
        str = [str temp];
        plot(theta,20*log10(abs(AFarr(phiphi,:)./max(AFarr(phiphi,:)))),'linewidth',1)
    end
    legend(str(2:end))
    ylim([-40 0])
    xlim([-80 80])
    xlabel('\theta [\circ]')
    ylabel('Magnitude [dB]')
    title('2D AF')
end


%3D plot
u = -1:0.1:1;
AFmatrix = zeros(length(u));
for v = -1:0.1:1
AFarrMAT = zeros(1,length(u));
for x = 0:(size(excite,2) - 1) %ch
    for y = 0:(size(excite,1) - 1) %brd
        AFarrMAT = AFarrMAT + (excite(y+1,x+1))*exp(1i*k*(x*d*(u-u0) + y*d*(v-v0)));
    end
end
AFmatrix(round(u,2,'significant') == round(v,2,'significant'),:) = AFarrMAT;
end
if plotindex
    figure
    hold on
    grid on
    surf(u,u,20*log10(abs(AFmatrix./max(max(AFmatrix)))))
    ylim([-1 1])
    xlim([-1 1])
    xlabel('u')
    ylabel('y')
    zlabel('Magnitude [dB]')
    title('3D AF')
end

end
```

B.3. Error model

```
function ErrorModel(Gapp,Papp,steer,theta,phi,f,Vin,Upattern)
%Example
%GG = 0.5;
%Gapp = [GG GG GG GG;
%        GG GG GG GG;
%        GG GG GG GG;
%        GG GG GG GG];
%
%Papp = [0 0 0 0;
%        0 0 0 0;
%        0 0 0 0;
%        0 0 0 0];
%
%steer = [0 0];
%theta = -80:80;
%phi = [90];
%f = 28;
%Vin = 0.01; %amplitude => -40dB <=> -10dBm

figure
hold on
```

```
grid on
for iter = 1:1e3

excite = zeros(4);
for brd = 1:4
    for ch = 1:4
        CH = (brd - 1)*4 + ch;
        [Mag, Phase] = newSDmodel(CH,f,Gapp(brd,5-ch),Papp(brd,5-ch));
        excite(brd,5-ch) = 10.^(Mag/20)*exp(1i*Phase) * Vin;
    end
end

[AFarr, ~] = BBoxAF(f*1e9,excite,theta,phi,steer(1),steer(2),0);

for a = 1:size(AFarr,1)
    plot(theta,20*log10(abs((AFarr(a,:)) .*Upattern)),'-b') %./max(abs(AFarr(a,:)))
end

end
xlabel('\theta [\circ]')
ylabel('Magnitude [dB]')
title('Error model and real Dome data')
end
```

Bibliography

[1] Verkotan, “Beamforming antenna’s - how they work and are tested,” (2022). [Online]. Available: https://verkotan.com/2021/beamforming-antennas-how-they-work-and-are-tested

[2] TMYTEK, “Datasheet, bbox™ one 28 ghz, bb-one-bp-28-(4x4/8x8),” Tech. Rep., (2021).

[3] J. P. Hoffmann, P. Leuchtmann, J. Schaub, and R. Vahldieck, “Computing uncertainties of s-parameters by means of monte carlo simulation,” in *2007 69th ARFTG Conference*, 2007, pp. 1–7.

[4] O. C. Ibe, “1 - basic concepts in probability,” in *Markov Processes for Stochastic Modeling (Second Edition)*, second edition ed., O. C. Ibe, Ed. Oxford: Elsevier, 2013, pp. 1–27. [Online]. Available: https://www.sciencedirect.com/science/article/pii/B9780124077959000013

[5] R. D. Yates and D. J. Goodman, *Probability and Stochastic Processes, 3rd ed*. John Wiley Sons Inc, (2014).

[6] TMYTEK, “bbox-api (version 3.3.13),” (2022). [Online]. Available: https://github.com/tmytek/bbox-api

[7] A. Froehlich and D. Hwang, “local area network (lan).” SearchNetworking, (2021).

[8] Keysight Technologies, “Agilent pna microwave network analyzers.” E8361A datasheet, (2014) [Revised May 2022].

[9] Teppati, V. Ferrero, A. Sayed, and Mohamed, *Modern RF and Microwave Measurement Techniques - 8.2 Error Model*. Cambridge University Press, (2013). [Online]. Available: https://app.knovel.com/hotlink/khtml/id:kt00C83Q91/modern-rf-microwave-measurement/error-model

[10] J.-H. Kim, J.-S. Kang, J.-I. Park, and C.-H. Cho, “Backward unknown-thru calibration method,” in *2020 95th ARFTG Microwave Measurement Conference (ARFTG)*, 2020, pp. 1–3. [Online]. Available: http://dx.doi.org/10.1109/ARFTG47271.2020.9241362

[11] F. Ferrara, C. Gennarelli, and R. Guerriero, *Near-Field Antenna Measurement Techniques*. Singapore: Springer Singapore, 2016, pp. 2107–2163. [Online]. Available: https://doi.org/10.1007/978-981-4560-44-3_117

[12] A. Ramírez-Arroyo, A. Alex-Amor, C. García-García, □. Palomares-Caballero, P. Padilla, and J. F. Valenzuela-Valdés, “Time-gating technique to emulate new scenarios,” in *2021 15th European Conference on Antennas and Propagation (EuCAP)*, 2021, pp. 1–5.

[13] A. Soltane, G. Andrieu, E. Perrin, C. Decroze, and A. Reineix, “Antenna radiation pattern measurement in a reverberating enclosure using the time-gating technique,” *IEEE Antennas and Wireless Propagation Letters*, vol. 19, no. 1, pp. 183–187, 2020.

[14] W. van Drongelen, “Chapter 6 - continuous, discrete, and fast fourier transform,” in *Signal Processing for Neuroscientists (Second Edition)*, second edition ed., W. van Drongelen, Ed. Academic Press, 2018, pp. 103–118. [Online]. Available: https://www.sciencedirect.com/science/article/pii/B9780128104828000060

[15] D. M. Carmine, “On-wafer near field antenna measurement,” Ph.D. dissertation, (2015).

[16] W. K. CHEN, “II - Antenna Elements and Arrays,” in *The Electrical Engineering Handbook*. Burlington: Academic Press, 2005, pp. 569–583. [Online]. Available: https://doi.org/10.1016/B978-012170960-0/50043-8

[17] H. Asplund, D. Astely, P. von Butovitsch, T. Chapman, M. Frenne, F. Ghasemzadeh, M. Hagström, B. Hogan, G. Jöngren, J. Karlsson, F. Kronestedt, and E. Larsson, "Chapter 4 - antenna arrays and classical beamforming," in *Advanced Antenna Systems for 5G Network Deployments*. Academic Press, 2020, pp. 89–132. [Online]. Available: https://doi.org/10.1016/B978-0-12-820046-9.00004-6

[18] L. Yepes, D. Covarrubias, M. Alonso, and J. Arceo, "Synthesis of two-dimensional antenna array using independent compression regions," *IEEE Transactions on Antennas and Propagation*, vol. 61, pp. 449–453, 12 2012.

[19] D. Kailash, "Study of broadside linear array antenna with different spacing and number of elements," *International Journal of Advanced Engineering Research and Science*, vol. 4, pp. 190–194, 01 2017.

[20] H. Ward, "Properties of dolph-chebyshev weighting functions," *IEEE Transactions on Aerospace and Electronic Systems*, vol. AES-9, no. 5, pp. 785–786, 1973.

[21] N. Fadlallah, L.Gargouri, A. Hammami, R. Ghayoula, A. Gharsallah, and B. Granado, "Antenna array synthesis with dolph-chebyshev method," 09 2011.